

Enhancement of Echo-Signal Correlation in Elastography Using Temporal Stretching

Tomy Varghese, *Member, IEEE*, and Jonathan Ophir

Abstract—Echo-signal decorrelation due to tissue compression is a significant source of error in tissue displacement estimates obtained using crosscorrelation. Tissue displacement estimates are used to compute strain values for imaging the elasticity of biological soft tissues. The correlation coefficient between the pre- and post-compression echo rf signals reduces rapidly with signal decorrelation due to increased compression. Miniscule reductions in the value of the correlation coefficient can have a significant impact on the performance of the strain estimator as illustrated by the strain filter. Reducing the rate of signal decorrelation using temporal stretching (which improves the value of the correlation coefficient), significantly improves the performance of the strain filter. The reduction in the rate of signal decorrelation with the subsequent increase in the correlation coefficient using temporal stretching is discussed in this paper. Theoretical, simulation and experimental results quantify the enhancement in the value of the correlation coefficient attained with temporal stretching.

I. INTRODUCTION

ULTRASONIC IMAGING of the elasticity of soft tissue is rapidly developing into a new diagnostic modality [1]–[5]. Some of the techniques for estimating tissue elasticity are based on strain estimation. Elastography, proposed by Ophir et al. [1], utilizes crosscorrelation analysis between the pre- and post-compression echo rf signal to estimate tissue displacements that are used in the computation of local strains. The range of applied strains in elastography is limited by the concomitant increase in echo-signal decorrelation [6]–[8]. Signal decorrelation is a significant source of error in the tissue displacement estimate, and methods to reduce it are of paramount importance.

Temporal stretching of the post-compression signal is one such method, which improves the correlation between the echo-signals, and thereby reduces the error in strain estimates [6]. The performance of the strain estimator in elastography has been quantified using a strain filter formulation [8]. The strain filter specifies the maximum signal-to-noise ratio in the elastogram (SNR_e), sensitivity and dynamic range at a given resolution. Reliable estimates of the strain are obtained only for correlation coefficients larger than 0.93, as illustrated by the strain filter [8]. Reducing the rate of signal decorrelation using temporal

stretching [6] (which improves the value of the correlation coefficient), may therefore have a strong impact on the performance of the strain filter. The enhancement in the performance of the strain filter due to temporal stretching will be discussed in an additional paper. In this paper, theoretical and simulation results are used to illustrate the improvement in the value of the rf crosscorrelation coefficient with temporal stretching.

Experimental and simulation results in [9] show significant improvements in the SNR_e and dynamic range using temporal stretching. For small compressions with subsequent temporal stretching, the crosscorrelation function closely resembles the autocorrelation function [10]. The strain estimates obtained after stretching the post-compression signal are precise and uncorrelated estimates (since stretching causes both the pre- and the post-compression rf signals to become jointly stationary [10]), when compared to the case when stretching is not performed (jointly non-stationary signals).

Temporal stretching as applied to a target with uniform elasticity is discussed in this paper. However, for non-uniform targets an adaptive stretching technique is applied which will be discussed in a subsequent paper. The stretched post-compression signal is obtained by resampling the signal with a linear stretch factor. Although, temporal stretching is not the inverse transformation of the deformation process, it helps in the estimation of the time-delay since it aligns the rf peaks.

A theoretical analysis of the correlation between different linear transformations of tissue and the corresponding ultrasonic speckle motion was studied in [11], using pre-envelope crosscorrelation analysis with motion compensation. Increased signal decorrelation due to rotation and biaxial transformations in tissue elements is modeled by reduction in the value of the correlation coefficient.

In this paper, we investigate the improvements in signal correlation with temporal stretching. The analysis is performed for uniformly elastic media. In addition, we assume that decorrelation due to the lateral and elevational components of the strain are negligible when compared to signal decorrelation due to axial strain. The rf correlation coefficients with and without temporal stretching are derived in Section II. The simulation experiment is described in Section III. Theoretical and simulation results are compared and analyzed in Section IV. Experimental results using a homogenous phantom are presented in Section V. Finally, Section VI summarizes the contributions of this paper.

Manuscript received February 20, 1996; accepted July 17, 1996. This work was supported in part by NIH grants R01-CA38515, R01-CA60520, and P01-CA64579, and by a grant from Dasonics Corp., Santa Clara, CA.

The authors are with the Ultrasonics Laboratory, Department of Radiology, the University of Texas Medical School, Houston, TX 77030.

II. THEORY

Tissue is modeled as a collection of randomly distributed weak scattering centers that interact with the ultrasound pulse as it propagates through the tissue. The scattering particles are assumed to interact with the pulse only once (multiple scattering is neglected). The backscattered echo-signals (A-line) from the randomly distributed speckle scatterers before compression along the axial direction can be written as:

$$r_1(x) = s(x) * p(x) + n_1(x) , \quad (1)$$

where $s(x)$ is the scattering function of the elastic tissue scattering particles, $p(x)$ is the impulse response of the system, $n_1(x)$ denotes the uncorrelated random noise, and $*$ denotes the convolution operation. The scattering particles move in all the three directions (axial, lateral and elevational) when the compressive force is applied. The echo-signal after compression along the axial direction (assuming that the tissue displacement along the lateral and elevational directions are small when compared to the axial displacement) can be written as:

$$r_2(x) = s\left(\frac{x}{\alpha}\right) * p(x) + n_2(x) , \quad (2)$$

where the subscripts $_1$ and $_2$ indicate the pre- and post-compression echo-signals obtained from an uniformly elastic tissue medium respectively, and α is a constant which depends on the compression and is given by $\alpha = 1 - \epsilon$, where ϵ is the applied strain. The correlation coefficient at peak of the normalized crosscorrelation function (CCF) between the pre- and the post-compression signals is given by:

$$\rho_{12} = \frac{C_{12}}{\sqrt{R_{11}R_{22}}} , \quad (3)$$

where C_{12} is the peak value of the CCF, R_{11} and R_{22} are the corresponding values of the autocorrelation functions.

To improve the correlation between the pre- and the post-compression signals, temporal stretching of the post-compression signal is performed. The post-compression signal is stretched by the factor by which the scatterers were compressed, yielding:

$$r_3(x) = s(x) * p(\alpha x) + n_3(x) , \quad (4)$$

where the subscript $_3$ denotes the temporally stretched post-compression rf signal. The corresponding peak value of the correlation coefficient between the pre- and the stretched post-compression signal can be written as:

$$\rho_{13} = \frac{C_{13}}{\sqrt{R_{11}R_{33}}} , \quad (5)$$

where R_{33} is the peak value of the autocorrelation function of the stretched post-compression signal.

In this paper, we will compare the improvement in the correlation coefficient obtained with temporal stretching.

The point-spread-function (PSF) of the pulse-echo imaging system and the tissue scattering function are defined in the next section. The correlation coefficients for both cases (with and without temporal stretching) are derived in the following sections.

A. Assumptions for the PSF

The one-dimensional PSF of the pulse-echo imaging system ($p(x)$) is modeled as a Gaussian modulated spatial cosine pulse, with wave number $k_o = \frac{2\pi}{\lambda_o}$, where λ_o is the wavelength of the ultrasound pulse, and a correlation length of σ , which determines the pulse width:

$$p(x) = \frac{1}{\sqrt{2\pi}\sigma} e^{-\left(\frac{x^2}{2\sigma^2}\right)} \cos(k_o x) . \quad (6)$$

Computation of the correlation coefficient for the Gaussian PSF is more tractable in the spectral domain. The Fourier transform of the PSF is given by:

$$P(u) = \frac{1}{2} \left(e^{-\left(\frac{(u+k_o)^2\sigma^2}{2}\right)} + e^{-\left(\frac{(u-k_o)^2\sigma^2}{2}\right)} \right) . \quad (7)$$

Meunier and Bertrand [11] consider only the first term in (7) (positive frequencies) for computing their motion compensated correlation coefficient value. The peak correlation coefficient before and after temporal stretching are computed in the following sections.

B. Correlation Coefficient Without Temporal Stretching

The CCF between the pre- and the post-compression echo rf signal at depths x_1 and x_2 is given by:

$$C_{12}(x_1, x_2) = E [r_1(x_1)r_2^*(x_2)] . \quad (8)$$

where $E[]$ denotes the expected value. The estimation problem in elastography is to determine the displacement $x_1 - x_2$, that produces the best alignment between the two echo-rf signals. This displacement estimate is determined by the correlation lag corresponding to the peak value of the CCF. Substituting (1) and (2) into (8) to obtain $C_{12}(x_1, x_2)$ in terms of the scattering function and the PSF:

$$C_{12}(x_1, x_2) = E \left[(s(x_1) * p(x_1) + n_1(x_1)) \left(s^* \left(\frac{x_2}{\alpha} \right) * p^*(x_2) + n_2^*(x_2) \right) \right] . \quad (9)$$

Since the noise terms ($n_1(x_1)$ and $n_2(x_2)$) in (9) are uncorrelated with each other and with the component due to the scatterers, (9) reduces to:

$$C_{12}(x_1, x_2) = E \left[(s(x_1) * p(x_1)) \left(s^* \left(\frac{x_2}{\alpha} \right) * p^*(x_2) \right) \right] . \quad (10)$$

The convolution term in (10) can be expressed as:

$$s(x_1) * p(x_1) = \frac{1}{2\pi} \int_{-\infty}^{+\infty} P(u_1) S(u_1) e^{ju_1 x_1} du_1 . \quad (11)$$

Using the formulation in (11), (10) reduces to:

$$C_{12}(x_1, x_2) = \frac{\alpha}{(2\pi)^2} \int_{-\infty}^{+\infty} \int_{-\infty}^{+\infty} P(u_1) P^*(u_2) E[S(u_1) S^*(\alpha u_2)] e^{j(u_1 x_1 - u_2 x_2)} du_1 du_2 . \quad (12)$$

The expected value in (12) is computed only over the scattering function since the terms due to the PSF is deterministic. If the scattering function is modeled as a white random noise process, the average cross spectrum of the noise process can be expressed as:

$$E[S(u_1) S^*(u_2)] = S \delta(u_1 - u_2) , \quad (13)$$

where $\delta(u_1 - u_2)$ is the Dirac delta function and S is the average energy of the tissue scattering function. Since the scattering function is real, the conjugate symmetry property, $S^*(u) = S(-u)$, is satisfied [12]. Substituting (13) into (12) and evaluating the integral over u_1 , we obtain:

$$C_{12}(x_1, x_2) = \frac{S\alpha^2}{(2\pi)} \int_{-\infty}^{+\infty} P(\alpha u_2) P^*(u_2) e^{ju_2(\alpha x_1 - x_2)} du_2 . \quad (14)$$

For the PSF defined in (6), the peak value of $C_{12}(x_1, x_2)$ reduces to:

$$C_{12} = \left(\frac{S\alpha^2}{4(2\pi)} \right) \left(\frac{2\sqrt{2\pi}}{\sigma\sqrt{\alpha^2 + 1}} \right) \left(e^{-\left(\frac{(\sigma k_o)^2 (1-\alpha)^2}{2(\alpha^2+1)}\right)} + e^{-\left(\frac{(\sigma k_o)^2 (1+\alpha)^2}{2(\alpha^2+1)}\right)} \right) . \quad (15)$$

A detailed derivation for (15) is presented in Appendix A for the cosine-modulated Gaussian PSF. The peak values of the autocorrelation function for the denominator in (3) are derived in a manner similar to (15) (see Appendix C for details), and are given by:

$$R_{11} = \left(\frac{S}{4(2\pi)} \right) \left(\frac{2\sqrt{\pi}}{\sigma} \right) \left(1 + e^{-(\sigma k_o)^2} \right) , \quad (16)$$

and

$$R_{22} = \left(\frac{S\alpha^2}{4(2\pi)} \right) \left(\frac{2\sqrt{\pi}}{\sigma\alpha} \right) \left(1 + e^{-(\sigma k_o)^2} \right) . \quad (17)$$

Using (3), the rf correlation coefficient peak value without temporal stretching can now be expressed as:

$$\rho_{12} = \left(\frac{\alpha\sqrt{2\alpha}}{(1 + e^{-(\sigma k_o)^2}) \sqrt{\alpha^2 + 1}} \right) \left(e^{-\left(\frac{(\sigma k_o)^2 (1-\alpha)^2}{2(\alpha^2+1)}\right)} + e^{-\left(\frac{(\sigma k_o)^2 (1+\alpha)^2}{2(\alpha^2+1)}\right)} \right) , \quad (18)$$

for $\alpha = 1$ (no tissue compression), the correlation coefficient $\rho_{12} = 1$ (best possible match between the pre- and the post-compression echo rf signal).

C. Correlation Coefficient with Temporal Stretching

The CCF between the pre- and the stretched post-compression echo rf signals at depths x_1 and x_2 , using (10) can be written as:

$$C_{13}(x_1, x_2) = E[(s(x_1) * p(x_1)) (s^*(x_2) * p^*(\alpha x_2))] . \quad (19)$$

Using the formulation of (11), (19) can be expressed as:

$$C_{13}(x_1, x_2) = \frac{1}{(2\pi)^2 \alpha} \int_{-\infty}^{+\infty} \int_{-\infty}^{+\infty} P(u_1) P^*\left(\frac{u_2}{\alpha}\right) E[S(u_1) S^*(u_2)] e^{j(u_1 x_1 - u_2 x_2)} du_1 du_2 . \quad (20)$$

We use the conjugate symmetry property of the scattering function. Substituting (13) in (20) and evaluating the integral over u_1 , we obtain:

$$C_{13}(x_1, x_2) = \frac{S}{(2\pi)\alpha} \int_{-\infty}^{+\infty} P(u_2) P^*\left(\frac{u_2}{\alpha}\right) e^{ju_2(x_1 - x_2)} du_2 . \quad (21)$$

For the pulse-echo PSF defined in (6), the peak value of $C_{13}(x_1, x_2)$ reduces to:

$$C_{13} = \left(\frac{S}{4(2\pi)\alpha} \right) \left(\frac{2\alpha\sqrt{2\pi}}{\sigma\sqrt{\alpha^2 + 1}} \right) \left(e^{-\left(\frac{(\sigma k_o)^2 (1-\alpha)^2}{2(\alpha^2+1)}\right)} + e^{-\left(\frac{(\sigma k_o)^2 (1+\alpha)^2}{2(\alpha^2+1)}\right)} \right) . \quad (22)$$

The peak value of the autocorrelation function for the stretched post-compression echo signal (derived using the same procedure followed in Appendix C) is given by:

$$R_{33} = \left(\frac{S}{4(2\pi)\alpha^2} \right) \left(\frac{2\alpha\sqrt{\pi}}{\sigma} \right) \left(1 + e^{-(\sigma k_o)^2} \right) . \quad (23)$$

Using (5), the rf correlation coefficient with temporal stretching can now be expressed as:

$$\rho_{13} = \left(\frac{\sqrt{2\alpha}}{(1 + e^{-(\sigma k_o)^2}) \sqrt{\alpha^2 + 1}} \right) \left(e^{-\left(\frac{(\sigma k_o)^2 (1-\alpha)^2}{2(\alpha^2+1)}\right)} + e^{-\left(\frac{(\sigma k_o)^2 (1+\alpha)^2}{2(\alpha^2+1)}\right)} \right) , \quad (24)$$

where $\rho_{13} = 1$ for $\alpha = 1$ (no tissue compression). Comparing (18) and (24), we observe the simple result that the correlation coefficient using temporal stretching differs from the correlation coefficient obtained without stretching by a factor of $1/\alpha$, namely:

$$\rho_{13} = \left(\frac{\rho_{12}}{\alpha} \right) . \quad (25)$$

Since $\alpha \leq 1$, $\rho_{13} \geq \rho_{12}$, this means that the stretching operation generally improves the correlation coefficient. This relationship between the correlation coefficient before and after temporal stretching holds for all values of α . We further use a relationship between signal-to-noise ratio (SNR) and the correlation coefficient, independently derived by Friemel [13] and Céspedes et al. [14]. Expressing the correlation coefficient before temporal stretching (ρ_{12}) in terms of an SNR , we obtain:

$$SNR_{12} = \frac{\rho_{12}}{1 - \rho_{12}} . \quad (26)$$

The correlation coefficient after temporal stretching, written as an SNR and expressed in terms of ρ_{12} (using (25)) is:

$$SNR_{13} = \frac{\rho_{12}/\alpha}{1 - \rho_{12}/\alpha} = \frac{1}{\alpha/\rho_{12} - 1} , \quad (27)$$

for small values of the compression $\alpha/\rho_{12} \approx 1$, which implies that $SNR_{13} \rightarrow \infty$. Therefore for small compressions, temporal stretching significantly improves the sonographic SNR by reducing signal decorrelation.

Theoretical plots of the peak value of the rf correlation coefficient function values before and after temporal stretching are plotted in Fig. 1 as a function of the applied strain. The graphs of the correlation coefficient represent a PSF with a standard deviation $\sigma = 0.154$ mm, and wave number = 20.4 mm^{-1} (corresponding to a 5 MHz center frequency). Note the improvement in the value of the correlation coefficient with temporal stretching. Signal decorrelation reduces with an increase in the pulse bandwidth, or a decrease in the axial duration of the pulse [11]. A simulation experiment is presented in the next section which corroborates the theoretical curves of the correlation coefficient.

III. METHOD

Theoretical results presented in the previous section are validated using a Monte-Carlo simulation using MATLAB. A-scans representing (1), (2) and (4), are simulated and their respective correlation coefficients computed over 100 independent realizations. The A-scans were simulated for a $1.3 \mu\text{s}$ (1 mm) duration with a 200 MHz sampling frequency. The speed of sound in tissue is assumed to be constant at 1540 m/s.

The PSF was simulated using a Gaussian modulated cosine pulse with a wave number = 20.4 mm^{-1} , and a 0.154 mm standard deviation. The scattering function consists of uniformly distributed point scatterers with density of 40 scatterers/pulse-width. The scatterer strengths are also uniformly distributed over the pulse-width. The scatterer density used in this experiment satisfies the requirement for fully developed speckle scatterers. The PSF is convolved with the scattering function to obtain the pre-compression A-scan.

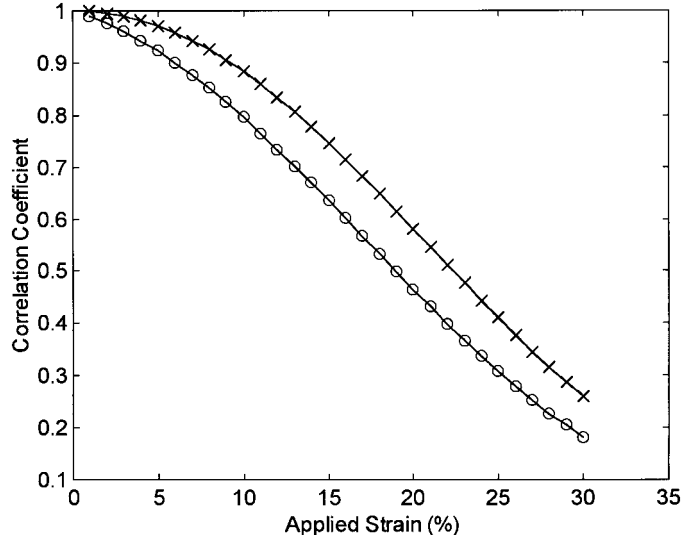


Fig. 1. Theoretical curves of the rf correlation coefficient, for a PSF with wave number = 20.4 mm^{-1} (corresponding to a 5 MHz center frequency), with a standard deviation = 0.154 mm for the Gaussian envelope. (a) Before temporal stretching (o o o). (b) After temporal stretching (x x x).

The displacement of the point scatterers due to the static compression, was derived by Céspedes [7] and Céspedes and Ophir in [6]. The applied stress is assumed to propagate uniformly so that the localized stress is constant throughout the medium of uniform elasticity. The displacement of each scatterer is a function of the applied strain and the position of the surrounding scatterers. The displacement of each scatterer is modeled by considering an equivalent one-dimensional spring system [6], [7]. The displacement (d_i) of the i^{th} scatterer due to a compression of Δy is given by:

$$d_i = \frac{\Delta y l_i}{L} , \quad (28)$$

where L is the length of the tissue medium, and l_i is the location of the i^{th} scatterer.

The post-compression A-scan (2) is obtained by convolving the PSF with the compressed point scatterers using (28). The stretched post-compression A-scan is simulated by convolving a stretched version of the PSF with the original scattering function using (4). In experiments on tissue phantoms, the stretched post-compression signal is obtained by temporally stretching the compressed rf-signal, which introduces additional noise in the rf signal due to signal interpolation used in the stretching process. In this paper, we illustrate the reduction in the signal decorrelation caused due to tissue compression using temporal stretching, and assuming negligible interpolation noise.

IV. RESULTS

The mean and standard deviation of the correlation coefficient estimates over 100 independent simulations are

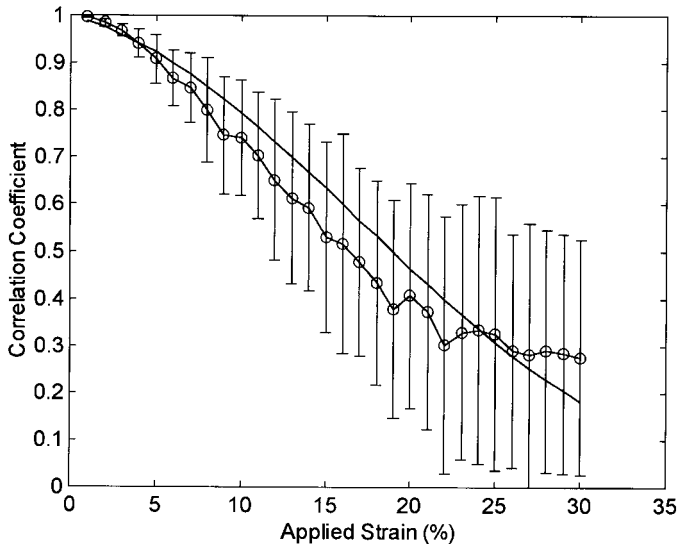


Fig. 2. Theoretical (—) and simulation (o o o) values of the correlation coefficient without temporal stretching, in a uniformly elastic simulated target, using a 1 mm data segment. The PSF used has a wave number = 20.4 mm^{-1} , with a standard deviation = 0.154 mm for the Gaussian envelope.

plotted in Fig. 2 and Fig. 3, with the standard deviation plotted as errorbars around the mean value of the correlation coefficient. Theoretical plots of the respective rf correlation coefficients are also presented along with the simulation results.

Figure 2 presents simulation and theoretical results for the variation of ρ_{12} with applied strain. The standard deviation of the correlation coefficient estimates are quite large (observe the length of the errorbars) over the entire range of applied strains as shown in Fig. 2. Notice the dramatic improvement in the rate of decorrelation of the simulations results and reduction in errorbar length with temporal stretching, as shown in Fig. 3. Temporal stretching not only improves the correlation coefficient, it also reduces the standard deviation for the range of applied strains currently used in elastography. However, the standard deviation progressively increases with applied strain as shown in Fig. 3. Temporal stretching is therefore extremely important, since it reduces signal decorrelation, a significant cause of noise in elastograms.

V. EXPERIMENTAL RESULTS

The elastography system consists of a Diasonics Spectra II scanner (Diasonics Inc., Santa Clara, CA) with a 5 MHz linear array, a digitizer (LeCroy Corp., Spring Valley, NY) operating at 48 MHz, a motion control system, and a compression device. A personal computer controls the operation of the entire system.

A homogenous gelatin phantom¹ that contains both speckle (graphite flakes) and resolvable scatterers (350 micron diameter glass beads) was used to obtain rf A-lines

¹Phantom was supplied courtesy of Dr. Timothy Hall.

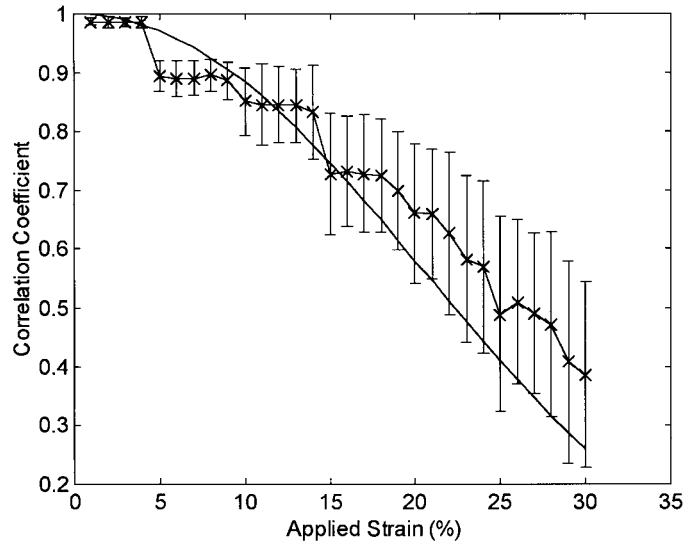


Fig. 3. Effect of temporal stretching of the post-compression signal in the value of the correlation coefficient. Theoretical (—) and simulation (x x x) results were obtained for a uniformly elastic simulated target, with a 1 mm data segment. Note the improvement in the value of the correlation coefficient for small strains when compared to Fig. 2.

before and after compression. A large compressor was used to simulate uniform stress conditions in the phantom. A single A-line along the axis of the compressor was used to compute the correlation coefficient before and after temporal stretching to minimize the effects of lateral and elevational signal decorrelation.

The peak of the normalized cross-correlation function was used to compute the value of the correlation coefficient. The correlation coefficient was computed over a 1 mm data segment ($1.3 \mu\text{s}$), with a 50% overlap between successive data segments. The post-compression rf signals were stretched by applying a linear stretch factor. The mean correlation coefficients over 100 estimates along with their standard deviations (error bars) are presented in Fig. 4. Note the significant improvement in the mean value of the correlation coefficient with temporal stretching. However, for large strains the correlation coefficient after temporal stretching approaches the correlation coefficient before stretching as observed in Fig. 4. This section illustrates the improvement in the value of the correlation coefficient obtained with temporal stretching and its application to experimental data.

VI. CONCLUSIONS

Signal decorrelation is a significant source of noise in elastograms. This paper analyzes the temporal stretching technique for reducing decorrelation noise. Theoretical simulation and experimental results in this paper illustrate the reduction in signal decorrelation obtained using temporal stretching. Small improvements in the rate of signal decorrelation have a significant impact on the performance of the strain filter [8], which improves the

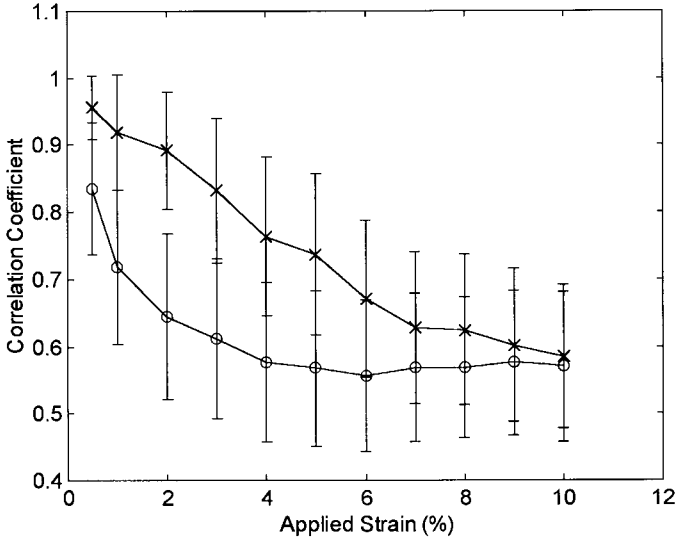


Fig. 4. Correlation coefficients obtained experimentally using rf A-lines from a homogenous phantom before (o o o) and after temporal stretching (x x x). A single A-line along the axis of the compressor was used to minimize the effects of lateral decorrelation. Note the improvement in the mean value of the correlation coefficient obtained with temporal stretching.

elastographic SNR_e , sensitivity and dynamic range. These results can be used to predict the extent of signal decorrelation with strain and the subsequent improvement with temporal stretching.

A relationship between the correlation coefficients before and after temporal stretching for a Gaussian modulated PSF is derived in this paper. Small improvements in the value of the correlation coefficient obtained with temporal stretching improve the SNR significantly (see (26) and (27)). Performance enhancements obtained with temporal stretching using a Gaussian PSF can be easily computed using the relationship derived in (25).

ACKNOWLEDGMENTS

The authors gratefully acknowledge helpful discussions with Dr. Mehmet Bilgen and on the 3-D Gaussian model with Dr. Jean Meunier. The homogenous phantom used in the experimental section of this paper was supplied by Dr. Timothy Hall.

APPENDIX A

Derivation of the crosscorrelation function for the cosine-modulated Gaussian PSF:

After replacing u_2 with u , the expression for the cross-correlation function from (14) is written as:

$$C_{12}(x_1, x_2) = \frac{S\alpha^2}{(2\pi)} \int_{-\infty}^{+\infty} P(\alpha u) P^*(u) e^{ju(\alpha x_1 - x_2)} du \quad (\text{A-1})$$

The peak value of the CCF ($\alpha x_1 - x_2 = 0$) using the cosine modulated Gaussian PSF is given by:

$$C_{12} = \frac{S\alpha^2}{4(2\pi)} \int_{-\infty}^{+\infty} \left(e^{-\left(\frac{(\alpha u + k_0)^2 \sigma^2}{2}\right)} + e^{-\left(\frac{(\alpha u - k_0)^2 \sigma^2}{2}\right)} \right) \left(e^{-\left(\frac{(u + k_0)^2 \sigma^2}{2}\right)} + e^{-\left(\frac{(u - k_0)^2 \sigma^2}{2}\right)} \right) du \quad (\text{A-2})$$

(A-2) is obtained by substituting (7) into (A-1). Expanding the terms in (A-2) we obtain:

$$C_{12} = \frac{S\alpha^2}{4(2\pi)} \int_{-\infty}^{+\infty} \left(e^{-\left(\frac{(\alpha u + k_0)^2 \sigma^2}{2}\right)} e^{-\left(\frac{(u + k_0)^2 \sigma^2}{2}\right)} + e^{-\left(\frac{(\alpha u - k_0)^2 \sigma^2}{2}\right)} e^{-\left(\frac{(u + k_0)^2 \sigma^2}{2}\right)} + e^{-\left(\frac{(\alpha u + k_0)^2 \sigma^2}{2}\right)} e^{-\left(\frac{(u - k_0)^2 \sigma^2}{2}\right)} + e^{-\left(\frac{(\alpha u - k_0)^2 \sigma^2}{2}\right)} e^{-\left(\frac{(u - k_0)^2 \sigma^2}{2}\right)} \right) du \quad (\text{A-3})$$

Integrating the four product terms in (A-3) as shown in Appendix B, we obtain:

$$C_{12} = \left(\frac{S\alpha^2}{4(2\pi)} \right) \left(\frac{\sqrt{2\pi}}{\sigma\sqrt{\alpha^2 + 1}} \right) \left(e^{-\left(\frac{(\sigma k_0)^2 (1-\alpha)^2}{2(\alpha^2 + 1)}\right)} + e^{-\left(\frac{(\sigma k_0)^2 (1+\alpha)^2}{2(\alpha^2 + 1)}\right)} + e^{-\left(\frac{(\sigma k_0)^2 (1+\alpha)^2}{2(\alpha^2 + 1)}\right)} + e^{-\left(\frac{(\sigma k_0)^2 (1-\alpha)^2}{2(\alpha^2 + 1)}\right)} \right) \quad (\text{A-4})$$

Simplifying (A-4), we obtain:

$$C_{12} = \left(\frac{S\alpha^2}{4(2\pi)} \right) \left(\frac{2\sqrt{2\pi}}{\sigma\sqrt{\alpha^2 + 1}} \right) \left(e^{-\left(\frac{(\sigma k_0)^2 (1-\alpha)^2}{2(\alpha^2 + 1)}\right)} + e^{-\left(\frac{(\sigma k_0)^2 (1+\alpha)^2}{2(\alpha^2 + 1)}\right)} \right) \quad (\text{A-5})$$

(A-5) is the same as (15) in the main body of the paper.

APPENDIX B

Integration of (A-3) is shown for the first product term in the equation, which is expressed as:

$$C_{12} = \frac{S\alpha^2}{4(2\pi)} \int_{-\infty}^{+\infty} \left(e^{-\left(\frac{(\alpha u + k_0)^2 \sigma^2}{2}\right)} e^{-\left(\frac{(u + k_0)^2 \sigma^2}{2}\right)} \right) du \quad (\text{B-1})$$

The product of the exponents within the integral can be expressed as:

$$C_{12} = \frac{S\alpha^2}{4(2\pi)} \int_{-\infty}^{+\infty} \left(e^{-\left(\frac{\sigma^2}{2}((\alpha u + k_o)^2 + (u + k_o)^2)\right)} \right) du . \quad (\text{B-2})$$

Completing the square within the exponent, reduces (B-2) to:

$$C_{12} = \frac{S\alpha^2}{4(2\pi)} \quad (\text{B-3})$$

$$\int_{-\infty}^{+\infty} \left(e^{-\left(\frac{\sigma^2(1+\alpha^2)}{2}\left(u + \frac{k_o(1+\alpha)}{1+\alpha^2}\right)^2\right)} e^{-\left(\frac{\sigma^2 k_o^2(1-\alpha)^2}{2(1+\alpha^2)}\right)} \right) du . \quad (\text{B-4})$$

Only the first term in (B-3) depends on u , integrating this term we obtain:

$$C_{12} = \left(\frac{S\alpha^2}{4(2\pi)} \right) \left(\frac{\sqrt{2\pi}}{\sigma\sqrt{\alpha^2+1}} \right) \left(e^{-\left(\frac{(\sigma k_o)^2(1-\alpha)^2}{2(\alpha^2+1)}\right)} \right) . \quad (\text{B-5})$$

which represents the first term in (A-4).

APPENDIX C

The value of the autocorrelation function at depths x_1 and x_2 for the pre-compression echo rf signal is given by:

$$R_{11}(x_1, x_2) = E[r_1(x_1)r_1^*(x_2)] . \quad (\text{C-1})$$

Substituting (1) into (C-1), we obtain:

$$R_{11}(x_1, x_2) = E[(s(x_1) * p(x_1))(s^*(x_2) * p^*(x_2))] . \quad (\text{C-2})$$

(C-2) using the formulation in (11) can be written as:

$$R_{11}(x_1, x_2) = \frac{1}{(2\pi)^2} \int_{-\infty}^{+\infty} \int_{-\infty}^{+\infty} P(u_1)P^*(u_2) E[S(u_1)S^*(u_2)] e^{j(u_1 x_1 - u_2 x_2)} du_1 du_2 . \quad (\text{C-3})$$

We use the conjugate symmetry property of the scattering function. Substituting (13) in (C-3) and evaluating the integral over u_1 , we obtain:

$$R_{11}(x_1, x_2) = \frac{S}{(2\pi)} \int_{-\infty}^{+\infty} |P(u_2)|^2 e^{ju_2(x_1 - x_2)} du_2 . \quad (\text{C-4})$$

Replacing u_2 with u , and using the pulse-echo PSF defined in (6), the peak value of R_{11} reduces to:

$$R_{11} = \frac{S}{4(2\pi)} \quad (\text{C-5})$$

$$\int_{-\infty}^{+\infty} \left(e^{-((u+k_o)\sigma)^2} + e^{-((u-k_o)\sigma)^2} + 2e^{-(\sigma u)^2} e^{-(\sigma k_o)^2} \right) du . \quad (\text{C-6})$$

Integration of the exponential terms in (C-5), gives:

$$R_{11} = \left(\frac{S}{4(2\pi)} \right) \left(\frac{2\sqrt{\pi}}{\sigma} \right) \left(1 + e^{-(\sigma k_o)^2} \right) . \quad (\text{C-7})$$

(C-5) is the same as (15) in the main body of the paper.

REFERENCES

- [1] J. Ophir, E. I. Céspedes, H. Ponnekanti, Y. Yazdi, and X. Li, Elastography: a quantitative method for imaging the elasticity of biological tissues, *Ultrasonic Imaging*, vol. 13, pp. 111–134, 1991.
- [2] E. I. Céspedes, J. Ophir, H. Ponnekanti, N. Maklad, Elastography: elasticity imaging using ultrasound with application to muscle and breast *in vivo*, *Ultrasonic Imaging*, vol. 15 (2), pp. 73–88, 1993.
- [3] M. O'Donnell, A. R. Skovoroda, and B. M. Shapo, Measurement of arterial wall motion using Fourier based speckle tracking algorithms, *Proc. 1991 IEEE Ultras. Symp.*, pp. 1101–1104, 1991.
- [4] M. Bertrand, M. Meunier, M. Doucet, and G. Ferland, Ultrasonic biomechanical strain gauge based on speckle tracking, *Proc. 1989 IEEE Ultrason. Symp.*, pp. 859–864, 1989.
- [5] H. E. Talhami, L. S. Wilson, and M. L. Neale, Spectral tissue strain: A new technique for imaging tissue strain using intravascular ultrasound, *Ultrasound Med. Biol.*, vol. 20, no. 8, pp. 759–772, 1994.
- [6] E. I. Céspedes and J. Ophir, Reduction of image noise in elastography, *Ultrasonic Imaging* vol. 15, pp. 89–102, 1993.
- [7] E. I. Céspedes, Elastography: imaging of biological tissue elasticity, *Ph.D. Dissertation* University of Houston, 1993.
- [8] T. Varghese and J. Ophir, A theoretical framework for performance characterization of elastography: The strain filter, *IEEE Trans. Ultrason., Ferroelect., Freq. Contr.*, vol. 44, no. 1, pp. 164–172, 1997.
- [9] T. Varghese, J. Ophir, and E. I. Céspedes, Noise reduction in elastography using temporal stretching with multicompression averaging, *Ultrasound Med. Biol.* vol. 22, no. 8, pp. 1043–1052, 1996.
- [10] S. K. Alam and J. Ophir, Reduction of signal decorrelation from mechanical compression of tissues by temporal stretching., *Ultrasound Med. Biol.*, vol. 23, no. 1, 1997.
- [11] J. Meunier and M. Bertrand, Ultrasonic texture motion analysis: Theory and simulation, *IEEE Trans. Ultrason., Ferroelect., Freq. Contr.*, vol. 14, pp. 293–300, 1995.
- [12] M. Bilgen and M. F. Insana, Deformation models and correlation analysis in elastography, *J. Acoust. Soc. Am.*, vol. 99, pp. 3212–3224, 1996.
- [13] B. H. Friemel, Real-time ultrasonic two-dimensional vector velocity estimation utilizing speckle-tracking algorithms: Implementation and limitations, *Ph.D. Dissertation*, Duke University, 1994.
- [14] E. I. Céspedes, J. Ophir, and S. K. Alam, The combined effect of signal decorrelation and random noise on time delay estimation, *IEEE Trans. Ultrason., Ferroelect., Freq. Contr.*, vol. 44, no. 1, pp. 220–225, 1997.



Tomy Varghese (S'92–M'95) received the B.E. degree in instrumentation technology from the University of Mysore, India, in 1988, and the M.S. and Ph.D. in electrical engineering from the University of Kentucky, Lexington, KY in 1992 and 1995, respectively. From 1988 to 1990 he was employed as an Engineer in Wipro Information Technology Ltd., India. He is currently a post-doctoral research associate at the Ultrasonics Laboratory, Department of Radiology, The University of Texas Medical School, Houston. His current research

interests include detection and estimation theory, statistical pattern

recognition, tissue characterization using ultrasound, and signal and image processing applications in medical imaging. Dr. Varghese is a member of the IEEE and Eta Kappa Nu.



Jonathan Ophir received his B.S.E.E. (summa cum laude), M.S.E.E., and Doctor of Engineering degrees from the University of Kansas, Lawrence Kansas in 1971, 1973, and 1977, respectively. His Doctoral dissertation describes an early implementation of digital scan conversion techniques for diagnostic ultrasound. During 1976–1977 he worked as a project engineer for Philips Ultrasound Inc., where he developed a commercial version of their first Digital Scan Converter. He then spent three years as an Assistant Professor of

Radiology at the University of Kansas Medical School in Kansas

City, where he was involved in the development of prototype sonographic contrast agents, ultrasound phantoms, and instrumentation for ultrasonic tissue characterization. From 1980 until the present time, he has been with the University of Texas Medical School at Houston, where he is currently Professor of Radiology. He is also Adjunct Professor of Electrical Engineering at the University of Houston. His current field of interest is elastography, the imaging of the elastic properties of soft tissues. Dr. Ophir has contributed more than 85 papers to peer-reviewed scientific journals, and holds 15 US and foreign patents. He is a Fellow of the American Institute of Ultrasound in Medicine, past Chairman of their standards committee, and past member of the board of governors. He is a member of the Editorial Board of *Ultrasound in Medicine and Biology*, and is Associate Editor of *Ultrasonic Imaging*. In 1992 he received the Terrence Matzuk Award from the American Institute of Ultrasound in Medicine, and in 1995 he was recognized as Inventor of the Year by the mayor of the city of Houston, Texas. In 1995 he also received an honorary commission as an Admiral in the Texas Navy by Governor George W. Bush.